HHS Public Access

Author manuscript

Nat Neurosci. Author manuscript; available in PMC 2017 August 06.

Published in final edited form as:

Nat Neurosci. 2017 March ; 20(3): 476–483. doi:10.1038/nn.4494.

Neuronal activity modifies the chromatin accessibility landscape in the adult brain

Yijing Su[1,2], **Jaehoon Shin**[1,2], **Chun Zhong**[1,2], **Sabrina Wang**[1], **Prith Roychowdhury**[1], **Jongseuk Lim**[1], **David Kim**[1], **Guo-li Ming**[1,2,3,4], and **Hongjun Song**[1,2,3]

[1]Institute for Cell Engineering, Johns Hopkins University School of Medicine, Baltimore, MD 21205, USA

[2]Department of Neurology, Johns Hopkins University School of Medicine, Baltimore, MD 21205, USA

[3]The Solomon H. Snyder Department of Neuroscience, Johns Hopkins University School of Medicine, Baltimore, MD 21205, USA

[4]Department of Psychiatry and Behavioral Sciences, Johns Hopkins University School of Medicine, Baltimore, MD 21205, USA

Abstract

Neuronal activity-induced gene expression modulates the function and plasticity of the nervous system. It is unknown whether and to what extent neuronal activity may trigger changes in chromatin accessibility, a major mode of epigenetic regulation of gene expression. Here we compared chromatin accessibility landscapes of adult mouse dentate granule neurons *in vivo* before and after synchronous neuronal activation using ATAC-seq. We found widespread, genome-wide changes one hour after activation, with enrichment of gained-open sites at active enhancer regions and at binding sites for AP1 complex components, including cFos. Some changes remain stable for at least twenty-four hours. Functional analysis further implicates a critical role of cFos in initiating, but not maintaining, neuronal activity-induced chromatin opening. Our results reveal dynamic changes of chromatin accessibility in the adult mammalian brain and suggest an epigenetic mechanism by which transient neuronal activation leads to dynamic changes in gene expression via modifying chromatin accessibility.

How transient activation of mature neuronal circuits leads to changes in gene expression and properties in neurons over the short and long-term is a fundamental question in neurobiology

Correspondence should be addressed to: Hongjun Song, Ph.D., Institute for Cell Engineering, Johns Hopkins University School of Medicine, 733 N. Broadway, MRB, 759, Baltimore, MD 21205, USA. Tel: 443-287-7499; Fax: 410-614-9568. shongju1@jhmi.edu.

GEO access number: GSE82015, GSE86367

A Supplementary Methods Checklist is available.

AUTHOR CONTRIBUTIONS: Y.S., H.S. designed the project. C.Z., prepared AAV virus and performed viral injections; Y.S., J.S., S.W., P.R., J.L. and D.K. contributed to data collection, analyses and interpretation. Y.S., J.S., G.M., and H.S. wrote the manuscript.

COMPETING FINANCIAL INTERESTS: The authors declare no competing financial interests.

Data availability: The data that support the findings of this study are available from the corresponding author upon request.

and has significant implications for understanding neuronal plasticity, learning and memory, and brain disorders[1]. Epigenetic mechanisms play a crucial role in regulating neuronal gene expression and neuronal activity is known to alter epigenetic landmarks, such as DNA methylation and histone modifications[2–11]. These epigenetic changes not only regulate which genes become activated or suppressed, but also modify the dynamics of gene expression[12].

Regulation of chromatin opening is an important regulatory mechanism for the precise control of gene expression patterns. Global changes in chromatin accessibility occur during cell differentiation when cells with an identical genome establish their identities through distinct gene expression patterns. Previous genome-wide studies of different tissues and cell types, including those in the nervous system, have revealed tissue- and cell type-specific landscapes of chromatin accessibility[13–16]. Whether large-scale changes in chromatin accessibility occur after cell differentiation and maturation *in vivo* is unclear. Specifically in the nervous system, whether and to what extent neuronal activity may reshape the accessible chromatin landscape in neurons and induce transient and sustained biological outcomes are largely unknown. Here we examined the impact of acute neuronal activation on chromatin accessibility and gene expression in dentate granule neurons over time in the adult mouse brain *in vivo.*

RESULTS

Widespread chromatin accessibility changes induced by neuronal activation

To investigate whether neuronal activation induces changes in chromatin accessibility, we employed an assay for transposase-accessible chromatin using sequencing (ATAC-seq) for sensitive and quantitative measurement of chromatin accessibility across the gemome[17] (See Methods). We performed ATAC-seq of biological replicates (n = 3 or 4 for each condition) of micro-dissected dentate gyri before (E0 thereafter) and 1 h (E1 thereafter) after synchronous neuronal activation via electroconvulsive stimulation[18–20], a procedure currently used to treat patients with drug-resistant depression[21]. Our previous studies have shown that this *in vivo* preparation is highly enriched for dentate granule neurons (over 90%) and such treatment switches most neurons from an inactive state that reflects the presumed sparse coding in the dentate gyrus[22], to an active state[18–20]. We identified 89,946 and 114,959 open chromatin regions at E0 and E1, respectively ($P < 1e\text{-}5$; Supplementary Table 1). We compared our dataset to previously published chromatin accessibility profiles of different tissues and cell types (Supplementary Table 2). The signature of open chromatin regions at the basal state (E0) is closer to those of different neuronal subtypes than astrocytes or other non neural tissues (Supplementary Fig. 1). We identified 16,882 open chromatin regions that occur in dentate gyrus neurons, but not in other cell types or tissues examined (Supplementary Table 3). Consistent with previous findings[13,23,24], open chromatin sites exhibited a broad genomic distribution, with the majority of peaks mapped to intergenic regions, introns and promoters of annotated genes (Supplementary Fig. 2a), and a positive correlation with the expression levels of associated genes (Supplementary Fig. 2b).

To determine how chromatin accessibility changes upon neuronal stimulation, we assessed quantitative differences in ATAC-seq signal intensity between E0 and E1. We observed

marked chromatin accessibility changes at many regions in multiple independent samples, such as “gained-open” at the *Arc* locus, which was correlated with induced gene expression, and “gained-closed” at the *Gabrr1* locus, which was correlated with diminished gene expression (Fig. 1a). ATAC-seq is based on the activity of Tn5[17]. To validate chromatin accessibility changes at the *Arc* and *Gabrr1* loci using an independent approach, we performed formaldehyde-assisted isolation of regulatory elements (FAIRE)-qPCR (Fig. 1b). Overall, ATAC-seq analysis identified 11,438 gained-open and 1,739 gained-closed regions at E1 compared to E0 ($P < 1e-5$; Fold changes > 2; Fig. 1c; Supplementary Table 4). Gene ontology (GO) analysis of 5,265 genes associated with “gained-open” regions revealed enrichment of pathways related to cell-cell signaling, synapses and synaptic transmission (Fig. 1d). Together, these results indicate that transient neuronal activation modifies the chromatin accessibility landscape in neurons *in vivo*, largely through increased accessibility.

Genomic features and chromatin states of regions with chromatin accessibility changes

To characterize the genome-wide distribution of activity-induced chromatin accessibility changes, we annotated those gained-open and gained-closed regions using HOMER[25]. The majority of changes resided outside of promoter regions of annotated genes (Fig. 2a), consistent with the ability of ATAC-seq to identify distal regulatory elements in the genome[17,26]. To determine the chromatin state of regions with activity-induced accessibility changes, we compared our differential chromatin accessibility dataset with published profiles of histone modifications from adult mouse hippocampus tissue[27] and a CTCF ChIP-seq dataset from the adult mouse cortex[28] (Supplementary Table 2). We observed overlap between gained-open regions and previously functionally identified enhancer regions[29–31] at the *Arc* and *cFos* loci (Supplementary Fig. 3a). Across the genome, active enhancer histone marks[32,33], such as H3K4me1 and H3K27ac, were more enriched at gained-open and gained-closed regions than transcription repressive markers[34,35], such as H3K27me3 and H3K9me3 (Fig. 2b; Supplementary Fig. 3b). To gain more detailed insight into the chromatin state of regions with accessibility changes, we used ChromHMM[36] to establish a chromatin state model defined by recurrent combinations of histone modifications using the ChIP-seq dataset from the adult mouse hippocampus[27] and CTCF ChIP-seq dataset from the adult mouse cortex[28]. Gained-open and gained-closed regions were found to be significantly enriched at active enhancers, as co-marked by H3K4me1 and H3K27Ac (Fig. 2c; Supplementary Fig. 3c). Chromatin accessibility changes also occurred near transcriptional start sites (TSS), as co-marked by H3K4me3 and H3K27ac (Fig. 2c and Supplementary Fig. 3c). We next asked whether chromatin accessibility is specifically correlated with histone modifications that are also sensitive to neuronal activity. We employed the published histone modification ChIP-seq dataset[32] from cultured neurons before and after KCl treatment, including H3K4me1, H3K4me3, H3K27ac and H3K27me3, and found that neither gained-open nor gained-closed regions were enriched in changes for those four histone marks (Supplementary Fig. 4).

To assess the potential biological significance of activity-induced chromatin accessibility changes, we first identified 4,455 and 558 genes that contained only gained-open or gained-closed regions at E1 compared to E0, respectively. We next performed RNA-seq analysis and identified 849 upregulated genes and 409 downregulated genes at E1 compared to E0 (*P*

< 0.05; Fold changes > 2; Fig. 2d; Supplementary Table 5). Comparison of these two datasets showed significant overlap of genes associated with gained-open peaks with upregulated genes (P = 9.7e-54), but not downregulated genes (P = 0.89; Fig. 2d). In addition, we found significant overlap of genes associated with gained-closed peaks with downregulated genes (P = 6.8e-4), but not with upregulated genes (P = 0.69; Fig. 2d). Together, these results indicate that neuronal activation leads to chromatin accessibility changes enriched at active enhancer regions, which in turn governs gene expression. Further, we observed that genes associated with chromatin opening are more likely to be upregulated, whereas genes associated with chromatin closing are more likely to be downregulated.

Role of cFos in activity-induced chromatin opening

Next we performed *de novo* motif analyses using MEME-ChIP[37] and HOMER[25] to identify transcription factors that are associated with regions with chromatin accessibility changes. The unbiased motif discovery analyses of gained-open regions identified a DNA logo with striking resemblance to the binding motif of the AP-1 complex, especially cFos, FosB and Jun subunits, which are classic neuronal activity-induced immediate-early genes[38] (P = 1.7e-1120; Fig. 3a; Supplementary Fig. 5a, c). About 78.9% of 11,438 gained-open regions at E1 contain the logo (Fig. 3b) and there is a significant overlap between gained-open regions and cFos ChIP-seq peaks[32] (P < 1e-6; Fig. 3c; Supplementary Table 6). Further genome-wide analysis revealed increased chromatin accessibility at binding sites for cFos, FosB and JunB, but not CREB, indicating specificity (Fig. 3d). In addition, there was increased ChIP signal for cFos, FosB and JunB, but not CREB, at activity-induced gained-open, but not gained-closed, regions (Fig. 3e). In contrast, the DNA logo identified using MEME-ChIP[37] and HOMER[25] for gained-closed regions does not match any know transcription factor binding motifs (P = 4.5e-51; Supplementary Fig. 5b–c).

Given that AP-1 subunits are well-known activity-induced immediate-early genes[39], the coincidence of AP-1 binding and neuronal activity-induced chromatin opening raises the possibility that AP-1 subunits play a functional role in chromatin opening. To test this hypothesis, we focused on cFos and first asked whether it is required for activity-induced chromatin opening at regions with cFos binding sites. We confirmed the induction of cFos expression in our experimental paradigm at both mRNA and protein levels (Supplementary Fig. 6a–b). We used a previously established AAV2/9 to co-express EYFP and shRNAs in the adult mouse dentate gyrus[20,40] (Supplementary Fig. 6c). Expression of shRNA against mouse cFos (shRNA-cFos), but not control shRNA (shRNA-Ctrl), effectively reduced neuronal activity-induced endogenous cFos expression as examined by Q-PCR and RNA-seq (Supplementary Fig. 6d, 7a). We performed ATAC-seq of dentate gyri expressing shRNA-Ctrl or shRNA-cFos at E0 and E1 (Fig. 4a–b; Supplementary Fig. 7b). Knockdown of cFos attenuated neuronal activity induced-chromatin opening at cFos-binding sites (Fig. 4a, c; Supplementary Fig. 7c; Supplementary Table 7). RNA-seq analysis further showed that activity-induced upregulation of genes associated with these sites was significantly attenuated (Fig. 4d; Supplementary Table 5). Notably, 72.1% of upregulated genes (P < 0.05; Fold changes > 2) in control neurons at E1 lost responsiveness in cFos knockdown neurons (Supplementary Fig. 7d). Together, these results suggest that cFos expression is required for

neuronal activity-induced chromatin opening at cFos-binding sites and subsequent upregulation of associated genes.

We next asked whether exogenous cFos expression in dentate granule neurons *in vivo* is sufficient to induce chromatin opening at cFos-binding sites. We used AAV to overexpress cFos and/or EYFP (Supplementary Fig. 6c, e) and performed ATAC-seq on dentate gyri in the absence of neuronal stimulation (Fig. 4a, e; Supplementary Table 7). Compared to EYFP expression alone, cFos overexpression partially mimics neuronal activity-induced chromatin opening at regions with cFos-binding sites (Fig. 4a, f). Among 647 chromatin gained-open regions induced by cFos overexpression, 56% overlapped with those induced by neuronal activity at E1 (Supplementary Fig. 7e). RNA-seq analysis further showed that genes associated with cFos-induced chromatin opening exhibited upregulated expression similar to that induced by neuronal activation (Fig. 4g). Together, these results support the model that neuronal activity-induced expression of the immediate-early gene cFos mediates chromatin opening at its binding sites, resulting in upregulated expression of associated genes.

Temporal characteristics of activity-induced neuronal chromatin accessibility changes

To evaluate whether neuronal activity-induced chromatin accessibility changes are sustained over time following a single stimulation, we additional performed ATAC-seq at 4 (E4) and 24 (E24) hours after synchronous neuronal activation (Supplementary Table 1). Comparison of datasets from different time points revealed many gained-open and gained-closed peaks at E4 and E24 compared to E0 (Fig. 5a–b; Supplementary Fig. 8a; Supplementary Table 4). Notably, 4,175 out of 11,438 (36.5%) activity-induced gained-open peaks at E1 remained open at E4, and 597 (5%) remained open till E24 (Fig. 5b, Supplementary Table 3). Overall, there are 517 genes associated with sustained gained-open and 22 genes with sustained gained-closed peaks for 24 h (Fig. 5c; Supplementary Table 4). GO analysis of genes associated with sustained gained-open peaks until 24 h revealed enrichment of pathways related to axon guidance, cell signaling and cell adhesion (Fig. 5d). Similar to E1, the majority of changes at E4 and E24 were distributed across the genome, mostly in introns and intergenic regions (Supplementary Fig. 8b, c).

We also characterized the chromatin state on those sustained gained-open peaks at E4 and E24 using ChromHMM (Fig. 6a). Gained-open peaks sustained for 4 h are enriched at active enhancers and a subset are located near TSS, whereas gained-open peaks sustained for 24 h are more enriched at sites upstream of TSS (Fig. 6b). Comparison of RNA-seq data from E1 and E4 to E0 identified 114 upregulated genes and 58 downregulated genes at both E1 and E4 ($P < 0.05$; Fold changes >2; Fig. 6c). There is a significant overlap of genes associated with gained-open peaks sustained for 4 h with upregulated genes ($P = 8.2e\text{-}27$), but not with downregulated genes ($P = 0.68$; Fig. 6c). RNA-seq analysis at E24 revealed 15 genes upregulated at all three time points (E1, E4 and E24), 3 of which are associated with gained-open sites sustained for 24 h ($P = 3.8e\text{-}3$).

The *de novo* motif discovery analysis of gained-open peaks sustained at E4 and E24 revealed DNA logos that resemble the binding motif of AP-1 ($P = 5.1e\text{-}479$ for E4; $P = 5.4e\text{-}397$ for E24; Fig. 7a). Approximately 44.8% and 60.6% of those gained-open peaks sustained for 4 h and 24 h overlap with cFos binding sites, respectively (Fig. 7b). One

hallmark property of immediate-early genes is their transient expression[38]. Synchronous neuronal activity led to transient cFos protein expression at 1 h, which became barely detectable at 4 h (Supplementary Fig. 6b). We selected multiple sustained gained-open regions associated with different genes for confirmation using cFos ChIP-qPCR analyses. Indeed, we could detect a significant association of cFos at these genomic loci at E1, but not at E0 or E4 (Fig. 7c; Supplementary Fig. 9). Together, these results suggest a model that cFos is required for the initiation, but not the maintenance, of neuronal activity-induced chromatin opening of regions with cFos binding sites over time (Fig. 7d).

DISCUSSION

It is now well-established that activity-induced re-shaping of transcriptomes plays a fundamental role in regulating neuronal properties, synaptic plasticity, cognitive function, and in various brain disorders[2–8,41,42]. In addition to classic modes of epigenetic regulation via DNA and histone modifications, here we show that neuronal activity dynamically regulates the chromatin accessibility landscape in mature mammalian neurons *in vivo*. Genes associated with gained chromatin opening are enriched in pathways related to cell-cell signaling, synapses, and synaptic transmission. Future studies will address how physiological stimuli, such as those encountered during explicit learning tasks, will impact chromatin accessibility in individual neurons *in vivo*. The large ATAC-seq and RNA-seq datasets from dentate granule neurons *in vivo*, a relatively pure population of a single neuronal subtype in the adult mammalian brain[19], at several time points after synchronous neuronal activation can provide a useful resource for the neuroscience field and beyond.

Neuronal activity-induced gene expression is known to very dynamic. The most well-known activity-induced genes are a set of immediate-early genes that include cFos and cJun[38,39]. In the classic model, it is believed that these transcription factors are rapidly induced by neuronal activity and then removed to allow transient regulation of downstream gene expression via binding to their genomic binding sites. Our unbiased motif analysis revealed coincident AP-1 binding sites and neuronal activity-induced chromatin opening regions. Further gain- and loss-of-function analyses of the AP-1 subunit cFos suggested an important role of cFos in the induction, but not maintenance, of neuronal activity-induced chromatin opening. We propose a model that, in addition to direct and acute regulation of their target genes, transcription factors encoded by immediate early genes, such as cFos, can play an additional role as an epigenetic regulator to modify chromatin accessibility around a subset of their binding sites across the genome.

Our time course analysis of the neuronal chromatin accessibility landscape upon acute activation showed that around 36.5% of the gained-open regions at 1 h remained open until 4 h and 5.1% remained until at least 24 h, whereas 27.8% of the gained-closed regions at 1 h remained closed until 4 h and 1.3% remained until 24 h (Fig. 5). A previous study of the same preparation has shown that 31% activity-induced changes in CpG methylation at 4 h are maintained at 24 h[19]. Therefore, compared to CpG DNA modification, activity-induced chromatin accessibility changes are relatively transient and reversible in neurons *in vivo*. Comparison of our chromatin accessibility datasets with previously published ChIP-seq datasets for various histone modifications revealed the enrichment of neuronal activity-

induced chromatin accessibility changes on active enhancer regions. Furthermore, RNA-seq analysis showed a significant correlation between gained-opened/gain-closed regions and upregulation/downregulation of associated genes. Given a large number of genes associated with gained open and gained-close regions at different time point after acute neuronal activation, our study therefore suggests a potential mechanism for how transient neuronal activation leads to dynamic changes in the expression of different sets of neuronal genes over time.

ONLINE METHODS

Animals

Adult male, 8–10 week-old mice in the C57BL/6 background were housed in a standard facility. All animal procedures used in this study were performed in accordance with protocols approved by the Institutional Animal Care and Use Committee of Johns Hopkins University School of Medicine. Synchronous neuronal activation of dentate granule neurons *in vivo* was achieved via electroconvulsive stimulation, which was administered with 1.0 s stimuli (total duration) consisting of 100 Hz, 16–18 mA, 0.3 ms pulses delivered using a Ugo Basile ECT unit (Ugo Basile, Collegeville, model 57800) as previously described[18,19]. Sham mice were similarly handled in parallel without the electrical current delivery. Previous studies using western blot and immunostaining of the activated form of caspase (Caspase 3a) and phosphorylated ATM (ataxia telangiectasia mutated kinase) showed that such treatment does not cause any detectable damage[18]. For AAV-based genetic manipulation, the recombinant AAV vectors were serotyped with AAV2/9. High titers of engineered AAV2/9 virus were stereotaxically injected into adult mouse dentate gyrus as previously described[44,45]. One week after viral injection, animals were subject to sham or electroconvulsive stimulation. Dentate gyrus region was rapidly fresh dissected from adult mouse hippocampus under a dissection microscope. Previous studies have shown that such preparations are highly enriched with mature dentate granule neurons (~90% $NeuN^+$ neurons)[18].

DNA Constructs

Mouse cFos open reading frame was cloned from adult mouse dentate gyrus 1 h after neuronal activation. AAV gene delivery vectors were constructed by cloning the EF1a-Gene-WPRE and U6-shRNA-EYFP-WPRE cassette into an AAV backbone[20]. The following shRNA sequences were used: shRNA-Ctrl: 5′-GTTCAGATGTGCGGCGAGT-3′; shRNA-cFos: 5′-GCCTTTCCTACTACCATTC-3′. The efficacy of shRNA against mouse cFos was confirmed by Q-PCR using adult mouse dentate gyri after AAV-mediated expression, followed by electroconvulsive stimulation. The following sequence primers for qPCR were used: actin-Forward: 5′-TAGGCACCAGGGTGTGATGG-3′; actin-Reverse: 5′-CATGGCTGGGGTGTTGAAGG-3′; cFos-Forward: 5′-GGGAATGGTGAAGACCGTGTCA-3′; cFos-Reverse: 5′-GCAGCCATCTTATTCCGTTCCC-3′.

ATAC-seq library construction, sequencing, mapping and data analysis

Transposome assay was performed as previously described[17]. Around 50,000 nuclei from each dentate gyrus were used. Q-PCR was used to estimate of the number of additional cycles needed to generate products at 25% saturation. Typically, four to seven additional PCR cycles were added to the initial set of five cycles. The library was purified on AMPure XP beads (Beckman A63881), analyzed on an Agilent Bioanalyzer, and 50 bp paired-end sequencing was performed using Illumina HiSeq 2500 platform according to standard operating procedures. Sequencing reads were mapped to mouse genome assembly (mm9) from the UCSC genome browser (http://genome.ucsc.edu/) using Bowtie2[46]. Duplicate reads were marked and removed by PICARD Tools (http://broadinstitute.github.io/picard/). Open chromatin peaks were analyzed using MACS[47] software. Differential peaks between different conditions were generated by diffReps[48]. Significant overlap between two sets of genomic regions was tested using GAT[49]. HOMER[25] was used to annotate those peaks for motif discovery analysis. IGV[50], ngsplot[51] were used for visualization of raw intensities. Statistical analyses were performed using in house R script unless otherwise specified.

RNA-seq and data analyses

Total RNA was purified from adult mouse dentate gyrus of independent samples using Rneasy kit (Qiagen), Dnase I on-column digestion was performed to avoid genomic DNA contamination. Sequencing libraries were prepared using NEBNext Ultra RNA Library Prep kit for Illumina (E7530L) following manufacturer's protocol. Briefly, total RNA was poly-A tail selected and then heat fragmented. The fragmented RNA was reverse transcribed and the second strand was synthesized to make double stranded DNA. After end repair and 3′ adenylation, adapters for multiplexing were ligated to the end of double stranded DNA fragments. The ligation products were amplified and purified to generate Illumina compatible libraries. Sequencing was performed with 100bp-single or paired end sequencing by Illumina Hiseq 2500 or NextSeq 500. The raw reads were mapped to the mouse genome build mm9 using tophat[52]. Differential gene expression and downstream analyses were performed using cuffdiff[53] and custom R scripts.

ChIP-qPCR analysis

Chromatin immunoprecipitation analysis was performed as previously described[54]. Briefly, dentate gyri from mice (E0, E1, E4) were microdissected on ice and subjected to ChIP using anti-cFos antibody (Santa Cruz) following manufacturer's instruction. The following sequence primers for qPCR were used in PCR to detect the presence of specific DNA binding to cFos: *Nrxn3*-Forward: 5′-GGCCTTTGTGGAGAATGAGA-3′; *Nrxn3*-Reverse: 5′-TTGTGGCTGGCTCTGTATTG-3′; *Gria2*-Forward: 5′-GGTTTGTCCCAGGCTGACTA-3′; *Gria2*-Reverse: 5′-GCAGCCTTCCTTTCTCTGAC-3′; *Kcnj6*-Forward: 5′-ATTCAGCGTCTTTGGGTTTG-3′; *Kcnj6*-Reverse: 5′-GCCTTAGGCTGTGTCAGAGG-3′; *Kcnv2*-Forward: 5′-TTTGAACCATAGCACCGACA-3′; *Kcnv2*-Reverse: 5′-GACTGCGAGGGTGTTTTCTC-3′; *Hivep3*-Forward: 5′-CCCCCTCTCTTGAGTCAGTG-3′; *Kcnv2*-Reverse: 5′-

GTCTGGCAGAAAAGGCTGTC-3′; Nr3c1-Forward: 5′-CTGCACGGGATCTCATTTTTT-3′; Nr3c1-Reverse: 5′-GGAGTAAATGGGCAGATGGA-3′.

FAIRE-qPCR analysis

FAIRE was performed following the previously published protocol[55,56]. Briefly, micro-dissected dentate gyri were cross-linked with 1% formaldehyde for 5 min and stopped with 0.125 M glycine for 5 min. The washed pellets were resuspended and incubated for 10 min sequentially in 1 ml of buffer L1 (50 mM HEPES-KOH, pH 7.5, 140 mM NaCl, 1 mM EDTA, 10% glycerol, 0.5% NP-40, 0.25% Triton X-100, 1X protease inhibitor) at 4°C for 10 min, 1 mL buffer L2 (10mM Tris-HCl, pH 8.0, 200 mM NaCl, 1 mM EDTA, 0.5 mM EGTA, 1X protease inhibitor) at room temperature for 10 min, and 400 μl of buffer L3 for 10 min (10 mM Tris-HCl, pH 8.0, 100 mM NaCl, 1 mM EDTA, 0.5 mM EGTA, 0.1% Na-Deoxycholate, 0.5% N-lauroylsarcosine, 1X protease inhibitor). The lysates were sonicated in order to shear chromatin into DNA fragments of average 300–500 bp, then centrifuged at 14,000 g for 10 min to remove the cellular debris. Input samples were reverse cross-linked overnight at 65 °C. The FAIRE samples and reverse cross-linked input samples were subjected to three sequential phenol/chloroform/isoamyl alcohol (25/24/1) extractions. DNA was precipitated with ethanol, air-dried and dissolved in 100 ul of TE and treated with 1 μl of RNase A (10 mg/ml) for 1 h at 37 °C. Proteins were then digested by proteinase K at 55 °C for 1 h and the DNA was purified with QIAquick PCR Purification Kit (Qiagen) and eluted with 30 ul ddH2O. The following sequence primers for qPCR were used in PCR to validate the chromatin opening and closing at E0 and E1: Arc_1-Forward: 5′-TTTCTTAGGGAGCAGCTGGA-3′; Arc_1-Reverse: 5′-CTAACCAAAGGCAGCTGAGG-3′; Arc_2-Forward: 5′-CAAGAACCCCCTTTCCTCTC-3′; Arc_2-Reverse: 5′-GAAGGGTGTGAGTGGGCTAA-3′; Arc_3-Forward: 5′-CCATAGCTCCTCTGGGAACA-3′; Arc_3-Reverse: 5′-CCATAGCTCCTCTGGGAACA-3′; Arc_4-Forward: 5′-GATTTGGTGGCTGGTGTTCT-3′; Arc_4-Reverse: 5′-CCTCCCATGGCTCTTACTCA-3′; Arc_5-Forward: 5′-CGTTTACGAGGAGAGCCAAG-3′; Arc_5-Reverse: 5′-CTTGGGCTTCCAAACCATTA-3′; Gabrr1-Forward: 5′-CCATAGCTCCTCTGGGAACA-3′; Gabrr1-Reverse: 5′-CCATAGCTCCTCTGGGAACA-3′.

Learning combinatorial chromatin states

ChromHMM was used to learn combinatorial chromatin states[57]. ChromHMM was trained using all seven chromatin marks (H3K4me1, H3K4me3, H3K27Ac, H3K27me3, H3K9me3, H4K20me1, H3K36me3) and CTCF in virtual concatenation mode across all conditions. Reads from replicate data sets were pooled before learning the states. The ChromHMM parameters used are as follows: reads were shifted in the 5′ to 3′ direction by 100 bp; for each ChIP-seq data set, read counts were computed in non-overlapping 200-bp bins across the entire genome; each bin was discretized into two levels, 1 indicating enrichment, and 0 indicating no enrichment. The binarization was performed by comparing ChIP-seq read

counts to corresponding whole-cell extract control read counts within each bin and using a Poisson *P* value threshold of 1×10^{-4}. We trained several models with the number of states ranging from 12 to 25 states. We decided to use a 15-state model for all further analyses as it captured all the key interactions among the chromatin marks and a larger number of states did not capture more interactions. To assign biologically meaningful mnemonics to the states, we used the ChromHMM package to compute the overlap and neighborhood enrichments of each state relative to coordinates of known gene annotations. The trained model was then used to compute the posterior probability of each state for each genomic bin in each condition.

Western Blot Analysis

Cell extracts were obtained from dentate gyri by resuspension in RIPA buffer (150 mM NaCl, 1.0% IGEPAL CA-630, 0.5% sodium deoxycholate, 0.1% SDS, 50 mM Tris, pH 8.0, fresh added 1 mM PMSF) followed by 30 min incubation on ice. Protein concentration was detected by BCA. Equal amounts of protein from different samples were loaded and separated by SDS-PAGE gel and transferred to nitrocellulose membranes (GE Healthcare Life Science) for immunoblot analysis. Blots were incubated in blocking buffer (5% bovine milk and 0.1% Tween 20 in PBS, pH 7.4) for 1 h at room temperature and then in anti-cFos primary antibodies (Santa Cruz, sc-7202; 1:200) overnight at 4°C, washed in blocking buffer three times for 10 min each, and incubated in corresponding secondary antibodies at room temperature for 2 h. Membranes were stripped and re-blotted with mouse anti-Actin antibodies (Millipore, MAB1501; 1:3000) as loading control. Western blot images were analyzed by ImageJ (Supplementary Fig. 10). Statistical significance was determined by ANOVA.

Statistics

No statistical methods were used to pre-determine sample sizes but our sample sizes are similar to those generally employed in the field[18–20, 23–28]. No randomization and blinding were employed.

Supplementary Material

Refer to Web version on PubMed Central for supplementary material.

Acknowledgments

We thank members of Song and Ming laboratories for discussion, Kimberly Christian for comments, Y. Cai and L. Liu for technical support. This work was supported by NIH (R37NS047344 and P01NS097206 to H.S., R35NS097370 and R01MH105128 to G-l.M.), SFARI (Award 240011 to H.S.), The Dr. Miriam and Sheldon G. Adelson Medical Research Foundation (to G-l.M.) and The Brain and Behavior Research Foundation (to Y.S.).

References

1. Crick F. Memory and molecular turnover. Nature. 1984; 312:101. [PubMed: 6504122]
2. Graff J, Kim D, Dobbin MM, Tsai LH. Epigenetic regulation of gene expression in physiological and pathological brain processes. Physiol Rev. 2011; 91:603–649. [PubMed: 21527733]
3. West AE, Greenberg ME. Neuronal activity-regulated gene transcription in synapse development and cognitive function. Cold Spring Harb Perspect Biol. 2011; 3

4. Sweatt JD. The emerging field of neuroepigenetics. Neuron. 2013; 80:624–632. [PubMed: 24183015]
5. Descalzi G, et al. Epigenetic mechanisms of chronic pain. Trends Neurosci. 2015; 38:237–246. [PubMed: 25765319]
6. Lattal KM, Wood MA. Epigenetics and persistent memory: implications for reconsolidation and silent extinction beyond the zero. Nat Neurosci. 2013; 16:124–129. [PubMed: 23354385]
7. Meaney MJ, Ferguson-Smith AC. Epigenetic regulation of the neural transcriptome: the meaning of the marks. Nat Neurosci. 2010; 13:1313–1318. [PubMed: 20975754]
8. Borrelli E, Nestler EJ, Allis CD, Sassone-Corsi P. Decoding the epigenetic language of neuronal plasticity. Neuron. 2008; 60:961–974. [PubMed: 19109904]
9. Guo JU, Su Y, Zhong C, Ming GL, Song H. Emerging roles of TET proteins and 5-hydroxymethylcytosines in active DNA demethylation and beyond. Cell cycle. 2011; 10:2662–2668. [PubMed: 21811096]
10. Cholewa-Waclaw J, et al. The Role of Epigenetic Mechanisms in the Regulation of Gene Expression in the Nervous System. J Neurosci. 2016; 36:11427–11434. [PubMed: 27911745]
11. Weng YL, An R, Shin J, Song H, Ming GL. DNA modifications and neurological disorders. Neurotherapeutics : the journal of the American Society for Experimental NeuroTherapeutics. 2013; 10:556–567. [PubMed: 24150811]
12. Jaenisch R, Bird A. Epigenetic regulation of gene expression: how the genome integrates intrinsic and environmental signals. Nat Genet. 2003; 33(Suppl):245–254. [PubMed: 12610534]
13. Vierstra J, et al. Mouse regulatory DNA landscapes reveal global principles of cis-regulatory evolution. Science. 2014; 346:1007–1012. [PubMed: 25411453]
14. Schmid RS, et al. Core pathway mutations induce de-differentiation of murine astrocytes into glioblastoma stem cells that are sensitive to radiation but resistant to temozolomide. Neuro-Oncology. 2016; 18:962–973. [PubMed: 26826202]
15. Mo A, et al. Epigenomic Signatures of Neuronal Diversity in the Mammalian Brain. Neuron. 2015; 86:1369–1384. [PubMed: 26087164]
16. Shin J, Ming GL, Song H. Decoding neural transcriptomes and epigenomes via high-throughput sequencing. Nat Neurosci. 2014; 17:1463–1475. [PubMed: 25349913]
17. Buenrostro JD, Giresi PG, Zaba LC, Chang HY, Greenleaf WJ. Transposition of native chromatin for fast and sensitive epigenomic profiling of open chromatin, DNA-binding proteins and nucleosome position. Nat Methods. 2013; 10:1213–1218. [PubMed: 24097267]
18. Ma DK, et al. Neuronal activity-induced Gadd45b promotes epigenetic DNA demethylation and adult neurogenesis. Science. 2009; 323:1074–1077. [PubMed: 19119186]
19. Guo JU, et al. Neuronal activity modifies the DNA methylation landscape in the adult brain. Nat Neurosci. 2011; 14:1345–1351. [PubMed: 21874013]
20. Guo JU, Su Y, Zhong C, Ming GL, Song H. Hydroxylation of 5-methylcytosine by TET1 promotes active DNA demethylation in the adult brain. Cell. 2011; 145:423–434. [PubMed: 21496894]
21. Lisanby SH. Electroconvulsive therapy for depression. N Engl J Med. 2007; 357:1939–1945. [PubMed: 17989386]
22. Neunuebel JP, Knierim JJ. Spatial firing correlates of physiologically distinct cell types of the rat dentate gyrus. J Neurosci. 2012; 32:3848–3858. [PubMed: 22423105]
23. Thurman RE, et al. The accessible chromatin landscape of the human genome. Nature. 2012; 489:75–82. [PubMed: 22955617]
24. Frank CL, et al. Regulation of chromatin accessibility and Zic binding at enhancers in the developing cerebellum. Nat Neurosci. 2015; 18:647–656. [PubMed: 25849986]
25. Heinz S, et al. Simple combinations of lineage-determining transcription factors prime cis-regulatory elements required for macrophage and B cell identities. Mol Cell. 2010; 38:576–589. [PubMed: 20513432]
26. Davie K, et al. Discovery of transcription factors and regulatory regions driving in vivo tumor development by ATAC-seq and FAIRE-seq open chromatin profiling. PLoS Genet. 2015; 11:e1004994. [PubMed: 25679813]

27. Gjoneska E, et al. Conserved epigenomic signals in mice and humans reveal immune basis of Alzheimer's disease. Nature. 2015; 518:365–369. [PubMed: 25693568]
28. Shen Y, et al. A map of the cis-regulatory sequences in the mouse genome. Nature. 2012; 488:116–120. [PubMed: 22763441]
29. Pintchovski SA, Peebles CL, Kim HJ, Verdin E, Finkbeiner S. The serum response factor and a putative novel transcription factor regulate expression of the immediate-early gene Arc/Arg3.1 in neurons. J Neurosci. 2009; 29:1525–1537. [PubMed: 19193899]
30. Kim TK, et al. Widespread transcription at neuronal activity-regulated enhancers. Nature. 2010; 465:182–187. [PubMed: 20393465]
31. Kawashima T, et al. Synaptic activity-responsive element in the Arc/Arg3.1 promoter essential for synapse-to-nucleus signaling in activated neurons. Proc Natl Acad Sci U S A. 2009; 106:316–321. [PubMed: 19116276]
32. Malik AN, et al. Genome-wide identification and characterization of functional neuronal activity-dependent enhancers. Nat Neurosci. 2014; 17:1330–1339. [PubMed: 25195102]
33. Shlyueva D, Stampfel G, Stark A. Transcriptional enhancers: from properties to genome-wide predictions. Nat Rev Genet. 2014; 15:272–286. [PubMed: 24614317]
34. Young MD, et al. ChIP-seq analysis reveals distinct H3K27me3 profiles that correlate with transcriptional activity. Nucleic Acids Research. 2011; 39:7415–7427. [PubMed: 21652639]
35. Barski A, et al. High-resolution profiling of histone methylations in the human genome. Cell. 2007; 129:823–837. [PubMed: 17512414]
36. Ernst J, Kellis M. Discovery and characterization of chromatin states for systematic annotation of the human genome. Nat Biotechnol. 2010; 28:817–825. [PubMed: 20657582]
37. Machanick P, Bailey TL. MEME-ChIP: motif analysis of large DNA datasets. Bioinformatics. 2011; 27:1696–1697. [PubMed: 21486936]
38. Curran T, Morgan JI. Fos: an immediate-early transcription factor in neurons. J Neurobiol. 1995; 26:403–412. [PubMed: 7775973]
39. Nedivi E, Hevroni D, Naot D, Israeli D, Citri Y. Numerous candidate plasticity-related genes revealed by differential cDNA cloning. Nature. 1993; 363:718–722. [PubMed: 8515813]
40. Jang MH, et al. Secreted frizzled-related protein 3 regulates activity-dependent adult hippocampal neurogenesis. Cell Stem Cell. 2013; 12:215–223. [PubMed: 23395446]
41. De Rubeis S, et al. Synaptic, transcriptional and chromatin genes disrupted in autism. Nature. 2014; 515:209–215. [PubMed: 25363760]
42. Felling RJ, Song H. Epigenetic mechanisms of neuroplasticity and the implications for stroke recovery. Exp Neurol. 2015; 268:37–45. [PubMed: 25263580]
43. Ma W, Noble WS, Bailey TL. Motif-based analysis of large nucleotide data sets using MEME-ChIP. Nat Protoc. 2014; 9:1428–1450. [PubMed: 24853928]
44. Ge S, et al. GABA regulates synaptic integration of newly generated neurons in the adult brain. Nature. 2006; 439:589–593. [PubMed: 16341203]
45. Duan X, et al. Disrupted-In-Schizophrenia 1 regulates integration of newly generated neurons in the adult brain. Cell. 2007; 130:1146–1158. [PubMed: 17825401]
46. Langmead B, Salzberg SL. Fast gapped-read alignment with Bowtie 2. Nat Methods. 2012; 9:357–359. [PubMed: 22388286]
47. Zhang Y, et al. Model-based analysis of ChIP-Seq (MACS). Genome Biol. 2008; 9:R137. [PubMed: 18798982]
48. Shen L, et al. diffReps: detecting differential chromatin modification sites from ChIP-seq data with biological replicates. PLoS One. 2013; 8:e65598. [PubMed: 23762400]
49. Heger A, Webber C, Goodson M, Ponting CP, Lunter G. GAT: a simulation framework for testing the association of genomic intervals. Bioinformatics. 2013; 29:2046–2048. [PubMed: 23782611]
50. Robinson JT, et al. Integrative genomics viewer. Nat Biotechnol. 2011; 29:24–26. [PubMed: 21221095]
51. Shen L, Shao N, Liu X, Nestler E. ngs.plot: Quick mining and visualization of next-generation sequencing data by integrating genomic databases. BMC Genomics. 2014; 15:284. [PubMed: 24735413]

52. Trapnell C, Pachter L, Salzberg SL. TopHat: discovering splice junctions with RNA-Seq. Bioinformatics. 2009; 25:1105–1111. [PubMed: 19289445]

53. Trapnell C, et al. Transcript assembly and quantification by RNA-Seq reveals unannotated transcripts and isoform switching during cell differentiation. Nat Biotechnol. 2010; 28:511–515. [PubMed: 20436464]

54. Guo JU, et al. Distribution, recognition and regulation of non-CpG methylation in the adult mammalian brain. Nat Neurosci. 2014; 17:215–222. [PubMed: 24362762]

55. Giresi PG, Lieb JD. Isolation of active regulatory elements from eukaryotic chromatin using FAIRE (Formaldehyde Assisted Isolation of Regulatory Elements). Methods. 2009; 48:233–239. [PubMed: 19303047]

56. Simon JM, Giresi PG, Davis IJ, Lieb JD. Using formaldehyde-assisted isolation of regulatory elements (FAIRE) to isolate active regulatory DNA. Nat Protoc. 2012; 7:256–267. [PubMed: 22262007]

57. Ernst J, Kellis M. ChromHMM: automating chromatin-state discovery and Characterization. Nat Methods. 2012; 9:215–216. [PubMed: 22373907]

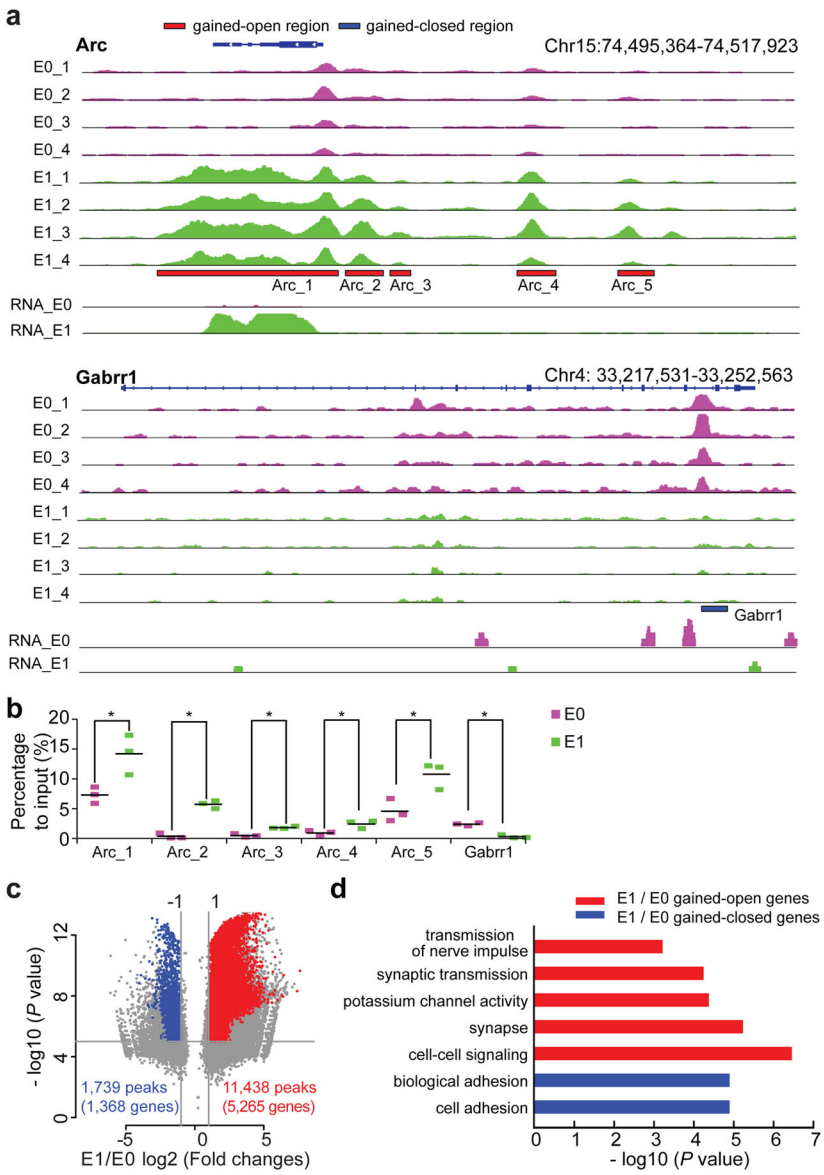

Figure 1.

Modification of the chromatin accessibility landscape in the adult mouse dentate gyrus by transient neuronal activation. (**a**) UCSC genome browser visualization of gained-open and gained-closed chromatin profiling coverage at the *Arc* and *Gabrr1* loci before (E0; magenta) and 1 h after synchronous neuronal activation (E1; green). Data from each individual sample are shown. Significant gained-open regions (red bars) and a gained-closed region (blue bar) are indicated ($P < 1e\text{-}5$; fold changes > 2). (**b**) Summary of FAIRE-qPCR results for gained-open and gained-closed regions at the *Arc* and *Gabbr1* loci. Data from three individual samples for each condition are shown (*$P < 0.05$; permutation test). (**c**) Comparison of open chromatin profiles of the dentate gyrus of adult mice between E1 and E0. Differential regions are shown in a volcano plot. Gained-open sites are shown in red and gained-closed sites are shown in blue ($P < 1e\text{-}5$; Fold changes > 2; T-test; n = 4 in each group). (**d**) GO

analysis of genes associated with gained-open (red) and gained-closed (blue) regions at E1 compared with E0.

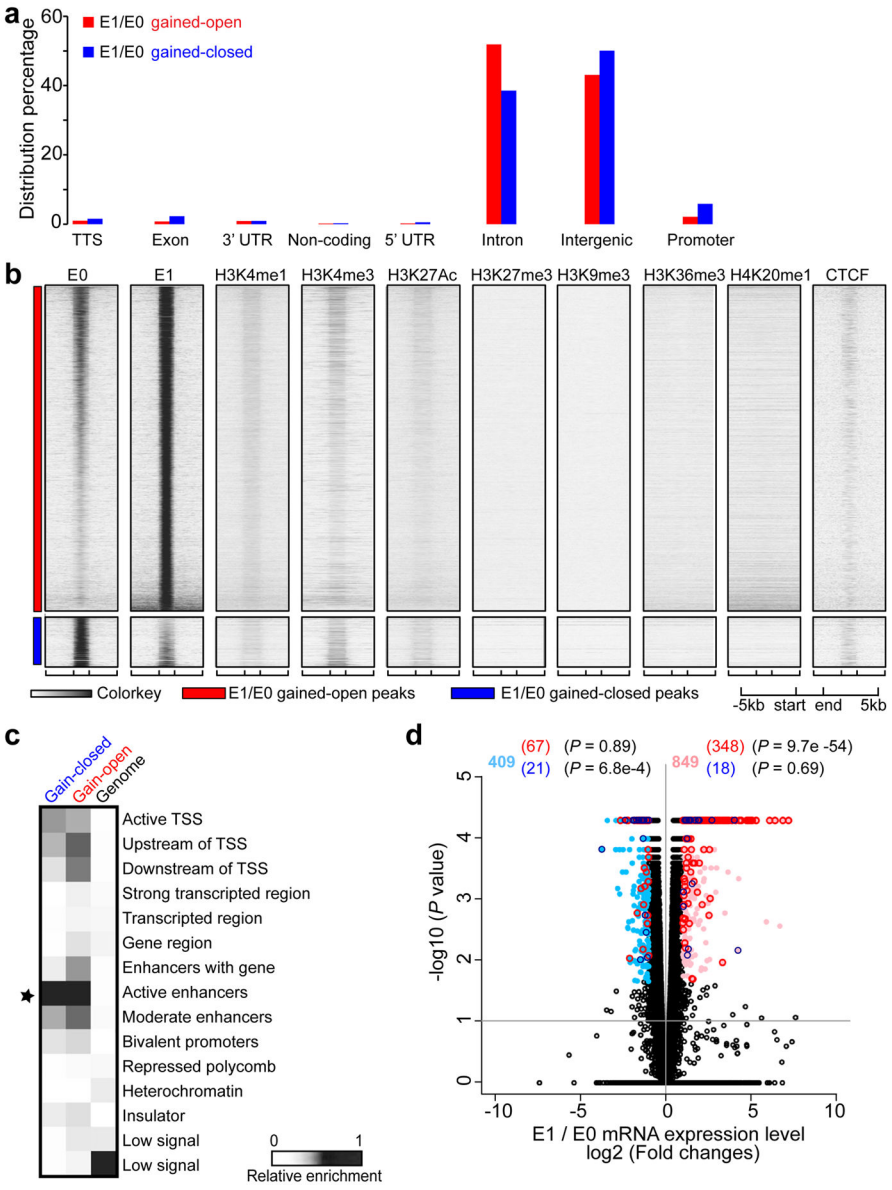

Figure 2.

Characterization of gained-open and gained-closed regions at E1 compared to E0. (**a**) Genomic features of gained-open (n = 11,438) and gained-closed regions (n = 1,739) at E1. (**b**) Genomic regions with neuronal activation-induced changes in chromatin accessibility are enriched with H3K4me1 and H3K27Ac active histone marks, but not with histone modifications for repressive (H3K27me3) markers. Regions between start and end define boundaries of differential sites. ChIP-seq mapped reads of various histone modifications[27] and CTCF[28] (see Supplementary Table 2 data sources) were plotted in heatmap views. (**c**) Characterization of histone modification states of gained-open and gained-closed regions using ChromHMM. The Star symbol highlights the most enrichment of gained-open and gained-closed regions are in active enhancers (**d**) Expression levels of genes associated with gained-open and gained-closed regions between E0 and E1. Significantly upregulated (pink)

and downregulated (light blue) genes between E1 and E0, and those overlapped with genes associated with gained-open peaks (red) or with genes associated with gained-closed peaks (blue) are coded in color ($P < 0.05$; Fold changes >2; Fisher's exact test).

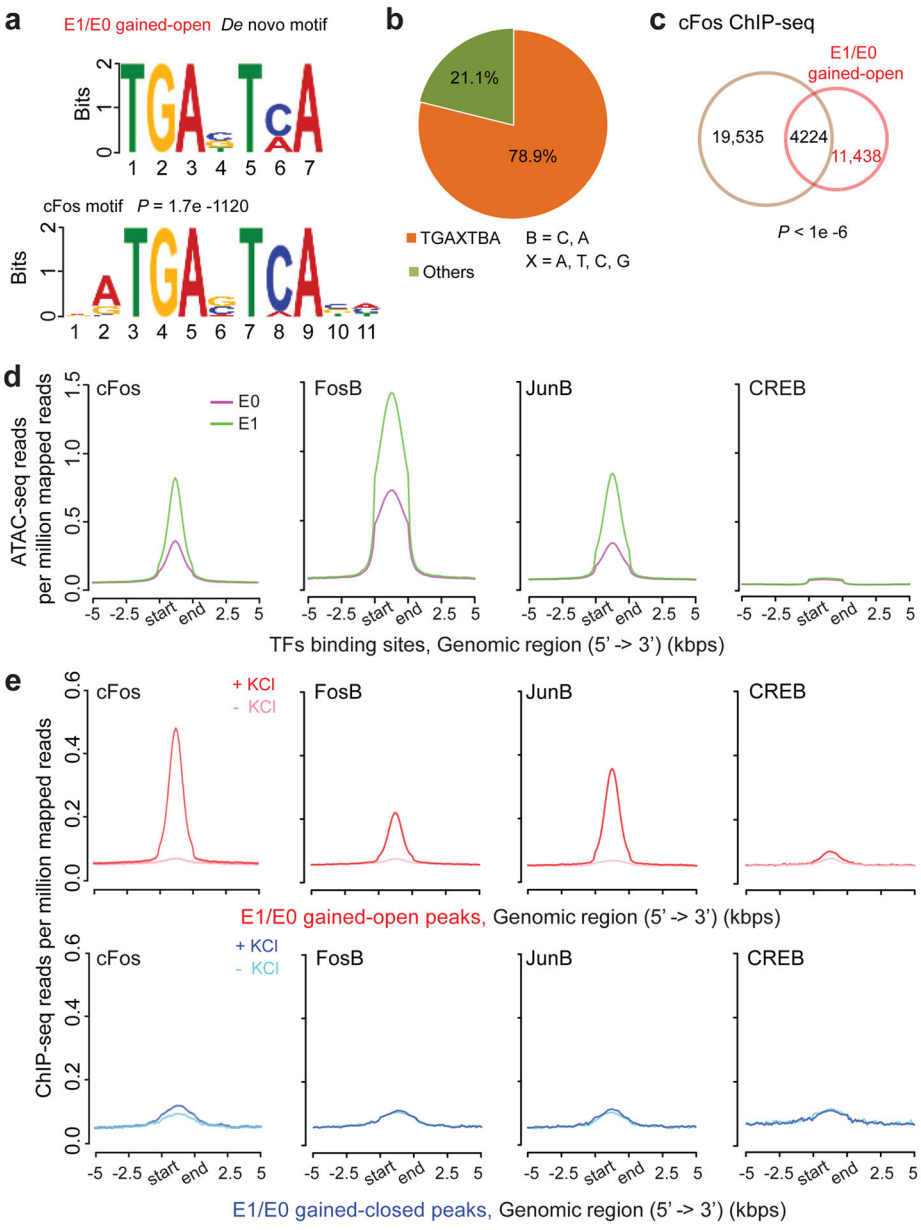

Figure 3.

Enrichment of cFos-binding sites at neuronal activity-induced chromatin opening regions. (**a**) Common motifs within chromatin gained-open regions at E1 (top) predicted using MEME-ChIP[43]. (**b**) Pie chart of gained-open peaks with the specific DNA logo. (**c**) Venn diagram of cFos ChIP binding sites and chromatin gained-open regions at E1. (**d**) Aggregate plots of ATAC-seq signals centered at cFos, FosB and JunB and CREB binding sites at E0 and E1. (**e**) Aggregate plots of cFos, FosB, JunB and CREB signals before and after KCl stimulation centered at gained-open (top panel) and gained-closed (bottom panel) sites at E1. The ChIP-seq data used for plots are from a previously published dataset[32].

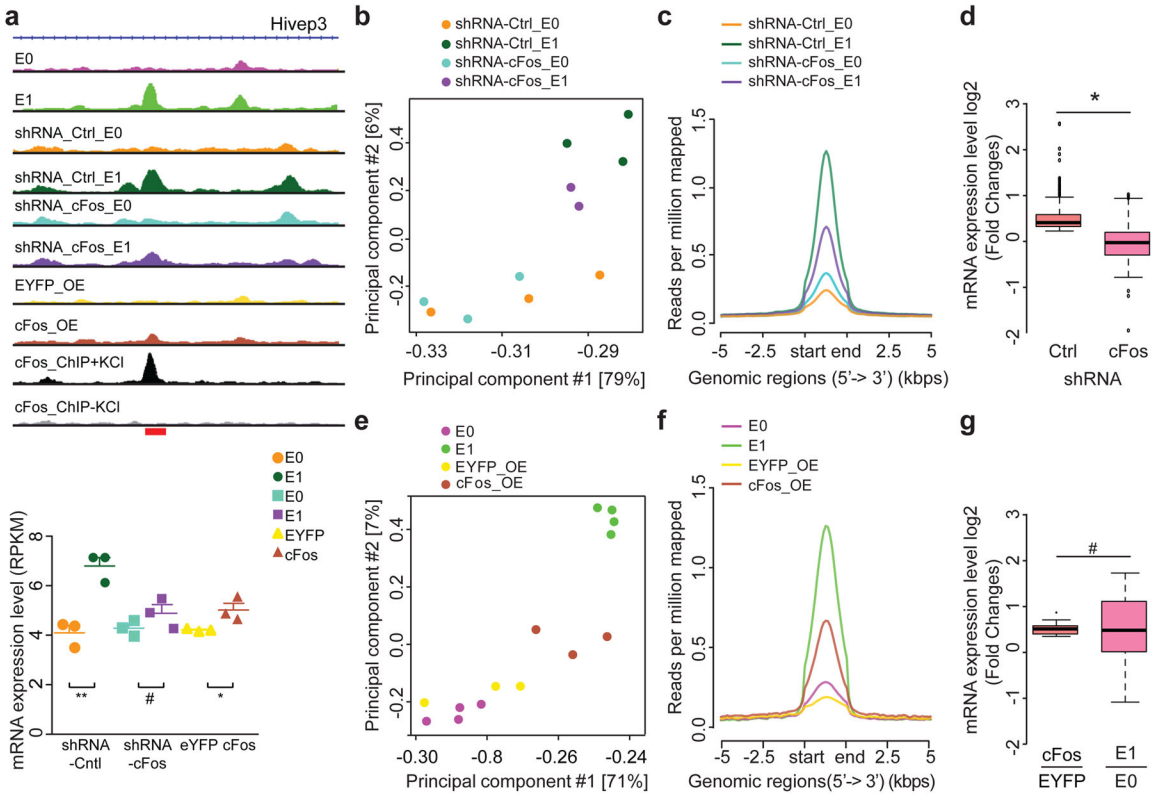

Figure 4.

Critical role of cFos in neuronal activity-induced chromatin opening of regions with cFos binding sites. (**a**) UCSC genome browser visualization of ATAC-seq profiles at the *Hivep3* locus under different conditions (top panels). Data from merged biological replicates (n = 2–3 mice in each group) are shown. Red bar indicates the region where cFos knockdown blocked activity-induced chromatin opening. Also shown is a plot of expression levels of *Hivep3* under different conditions (bottom panel; n = 3 mice in each groups; $*P < 0.05$; $**P < 0.01$; $^{\#}P > 0.1$; permutation test) (**b**) Principal component analysis of ATAC-seq of neurons expressing shRNA-Ctrl and shRNA-cFos at E0 and E1. (**c**) Aggregate plot of ATAC-seq signals centered on neuronal activity-induced gained-open regions with cFos-binding sites for neurons expressing shRNA-Ctrl and shRNA-cFos at E0 and E1. (**d**) Box-plot of mean expression levels of up-regulated genes in neurons expressing shRNA-Ctrl and shRNA-cFos in response to neuronal activation ($*P < 0.01$; Wilcoxon rank-sum test; $P < 2.2e\text{-}16$). Center line: median value; box limits: 25th and 75th percentile values; whiskers; maximum and minimum data points excluding the outliers; outliers: data points that are higher or lower than the 1.5 times the quartile (25th and 75th) values. (**e**) Principal components analysis of ATAC-seq of neurons expressing EYFP or cFos in the absence of neuronal stimulation. (**f**) Aggregate plot of ATAC-seq analysis of neurons at E0 and E1 and neurons overexpressing cFos (cFos-OE) and/or EYFP (EYFP-OE) at E0. Similar to (**c**). (**g**) Box-plot of mean expression levels of up-regulated genes induced by cFos expression at E0 or neuronal activation at E1 without exogenous cFos expression. Similar to (**d**) ($^{\#}P > 0.01$; Wilcoxon rank-sum test; $P = 0.81$).

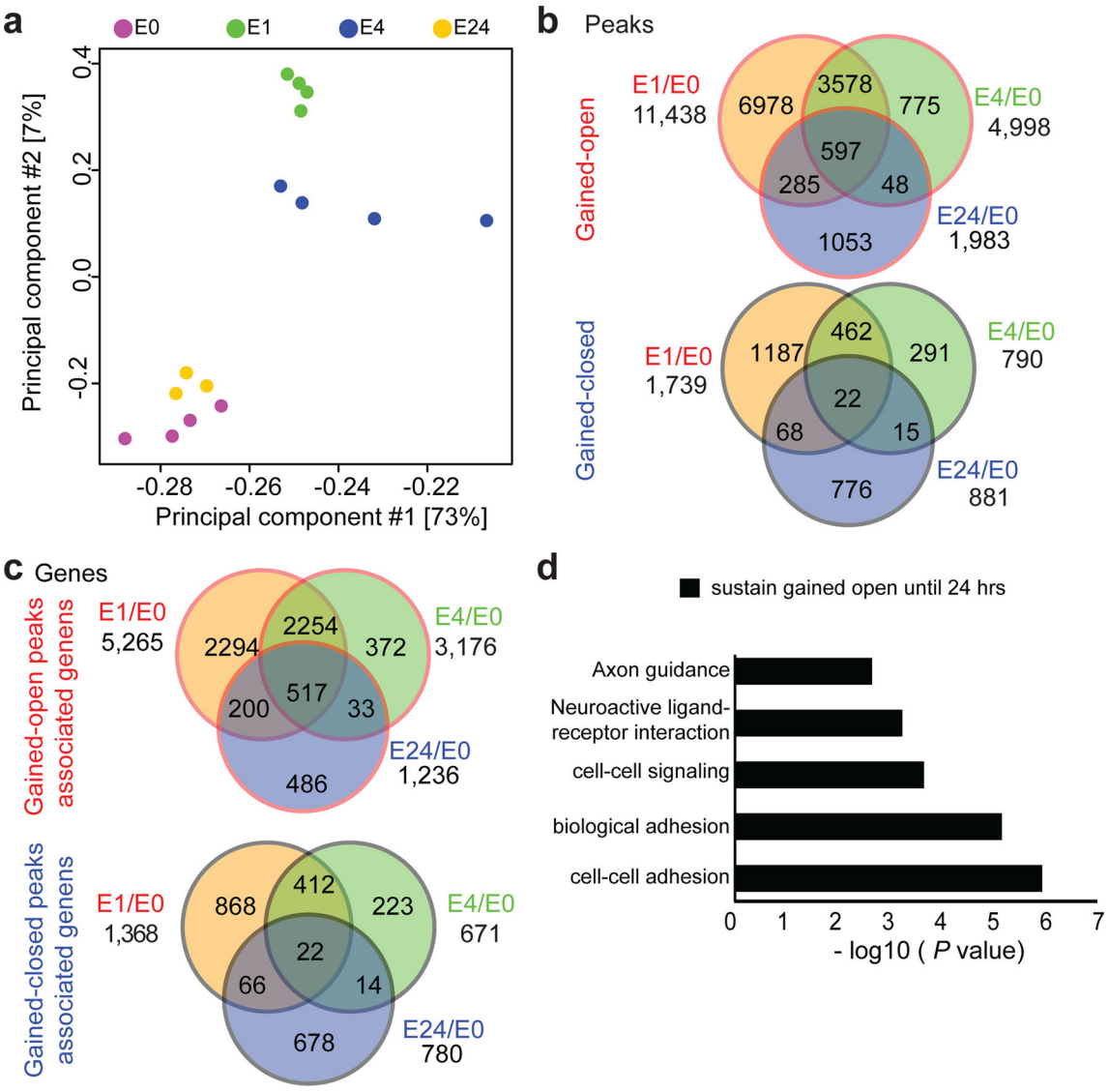

Figure 5.

Characterization of neuronal activity-induced chromatin accessibility changes at different time points. (**a**) Principal component analysis of ATAC-seq datasets. Each dot represents data from one sample and is colored coded for before (E0), 1 h (E1), 4 h (E4), or 24 h (E24) after synchronous neuronal activation. (**b, c**) Venn diagrams of differential chromatin accessible regions (**b**) and their associated genes (**c**). (**d**) GO analysis of genes with sustained gained-open chromatin accessibility until 24 h.

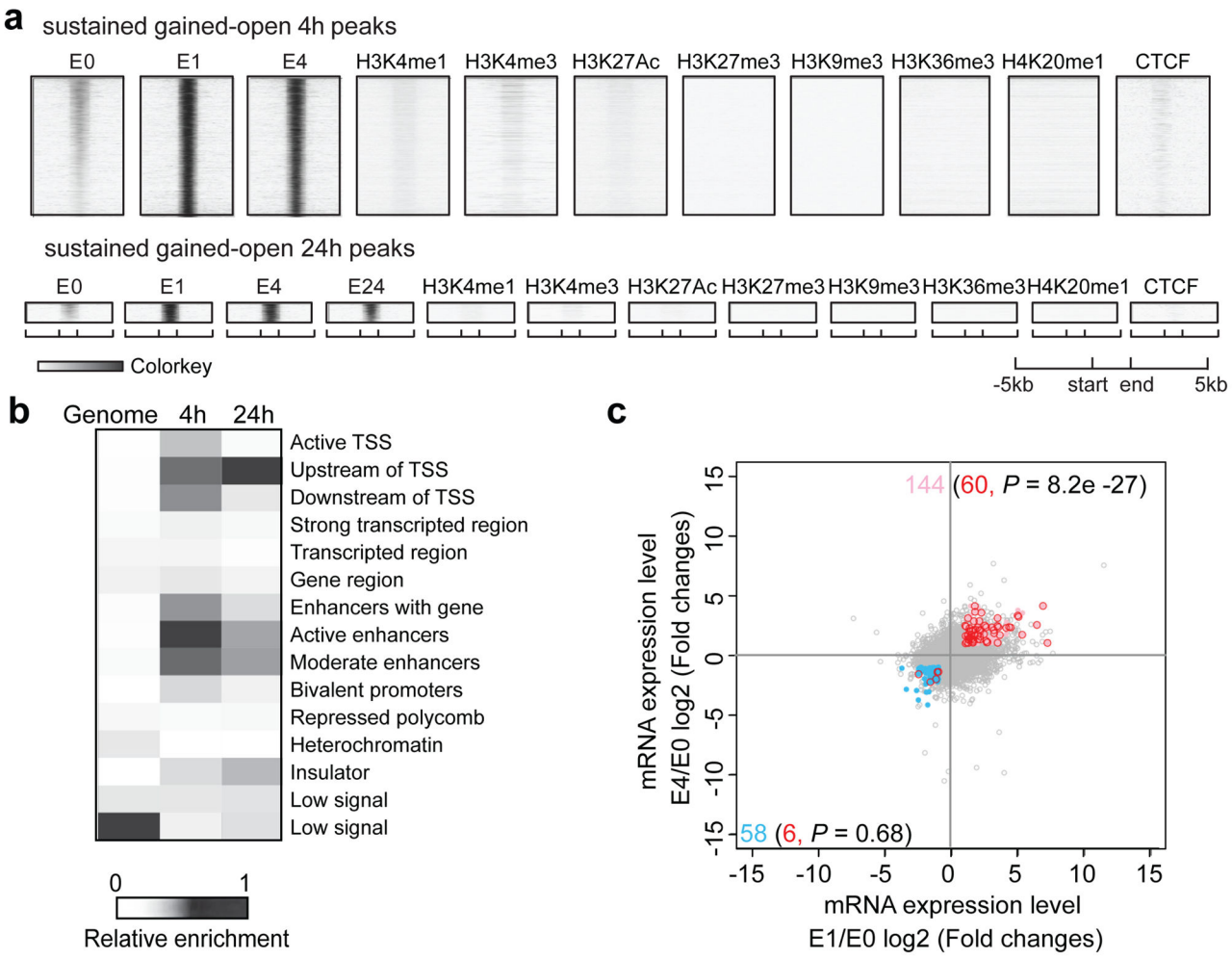

Figure 6.

Characterization of chromatin accessibility gained-open regions sustained for 4 h and 24 h. (**a**) Genomic regions with gained-opening sustained for 4 h and 24 h are enriched with H3K4me1 and H3K27Ac active histone marks, but not with histone modifications for repressive (H3K27me3) markers. Similar to Fig. 2b. (**b**) Characterization of histone modification states of gained-open regions sustained for 4 h and 24 h using ChromHMM. Similar to Fig. 2c. (**c**) Expression levels of genes associated with gained-open regions sustained for 4 h at E1 and E4. Significantly upregulated (pink) and downregulated (light blue) genes at both E1 and E4 compared to E0, and those overlapped with genes associated with gained-open peaks sustained for 4 h are coded in red ($P < 0.05$; Fold changes >2).

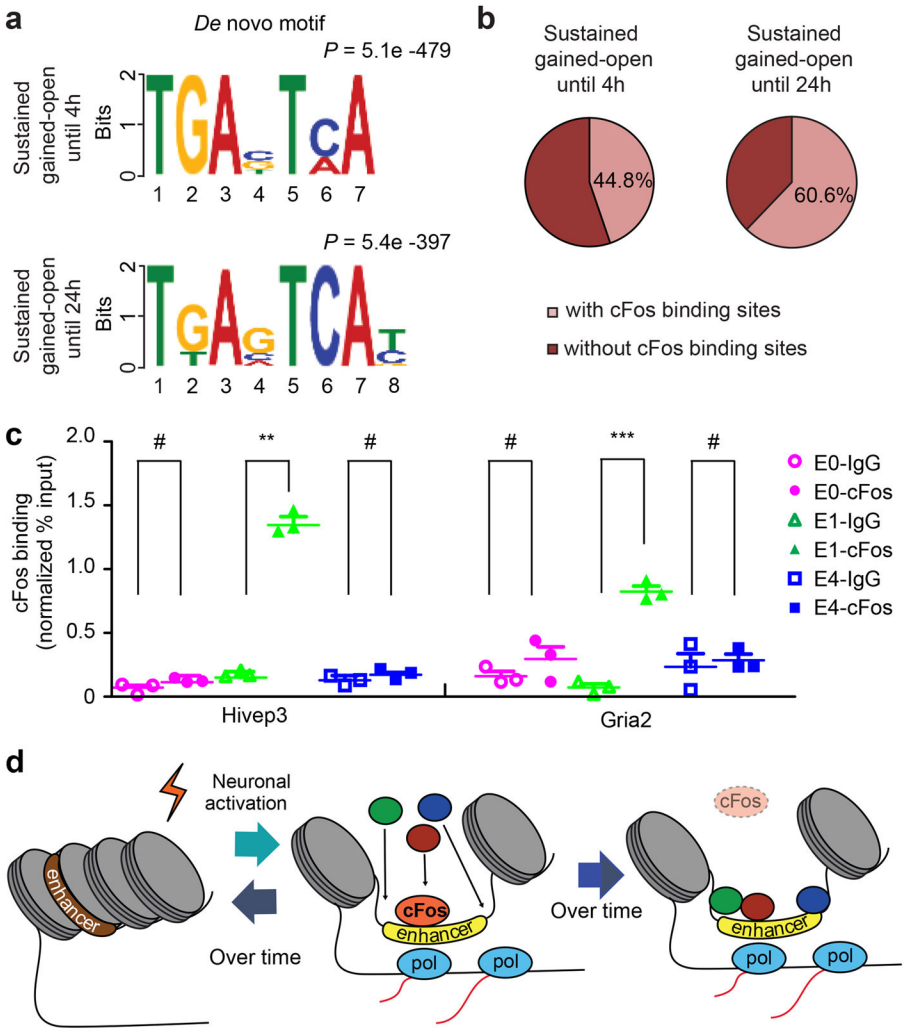

Figure 7.

Gained-open sites can be maintained without cFos occupation. (**a**) Common motifs within chromatin gained-open regions sustained for 4 h (top panel) and 24 h (bottom panel) predicted using MEME-ChIP[43]. (**b**) Pie chart of gained-open regions sustained for 4 h and 24 h with cFos-binding sites. (**c**) ChIP of cFos and IgG followed by qPCR analysis of *Hivep3* and *Gria2* loci in the adult dentate gyrus at E0, E4 and E24 (normalized percentage input). Data from individual samples are shown ($^{\#}P > 0.05$; permutation test). (**d**) A working model for neuronal activity-induced changes in chromatin accessibility and dynamic changes in neuronal gene expression over time.